Renewable Energy 106 (2017) 232–242

Contents lists available at ScienceDirect

Renewable Energy

journal homepage: www.elsevier.com/locate/renene

Novel fast and high accuracy maximum power point tracking method for hybrid photovoltaic/fuel cell energy conversion systems

Hassan Fathabadi

School of Electrical and Computer Engineering, National Technical University of Athens (NTUA), Athens, Greece

ARTICLE INFO

Article history:
Received 26 August 2016
Received in revised form
20 December 2016
Accepted 12 January 2017
Available online 18 January 2017

Keywords:
Maximum power point tracking
Hybrid system
Photovoltaic
Fuel cell

ABSTRACT

Currently, two maximum power point tracking (MPPT) units are used in hybrid photovoltaic (PV)/fuel cell (FC) systems, one for the PV subsystem and the other one for the FC stack, which significantly complicates the system implementation, and increases cost. This paper addresses this problem by presenting a novel fast and highly accurate unified MPPT technique for extracting maximum output power from hybrid PV/FC energy conversion systems. It is the only unified MPPT technique reported in the literature that uses a single algorithm to concurrently track the maximum power points (MPPs) of both PV module and FC stack used in a hybrid PV/FC system. A hybrid PV/FC energy conversion system has been built to evaluate the performance of the method. It is experimentally verified that the proposed MPPT method performs a very fast and highly accurate MPPT process, so that, the MPPT efficiency in the PV and FC subsystems is more than 99.60% and 99.41%, respectively, along with a very short convergence time of at most 12 ms and 33 s, respectively. Comparison between the MPPT method presented in this work and the state-of-the-art MPPT methods has been also performed that explicitly demonstrates the method has the highest MPPT efficiencies (99.60%, and 99.41%) along with the shortest convergence time (12 ms) compared to the state-of-the-art MPPT methods, while it concurrently performs two tasks (tracking two MPPs) but others perform only one task (tracking one MPP).

1. Introduction

Recently, there has been a rapid increase in the use of renewable energy resources, in particular, solar and wind energy [1,2], due to the problems such as reduction in fossil fuels availability and environmental issues. In practice, to increase rated power and reliability, renewable power sources are often combined with other power sources to arrange a hybrid energy conversion system such as a hybrid photovoltaic (PV)/fuel cell (FC) system [3]. A hybrid PV/FC system consists of a PV subsystem used as the main power source and a FC stack which is usually used as a standby power source. This configuration makes a hybrid PV/FC energy conversion system more reliable and applicable to industrial applications [4]. Currently, two maximum power point tracking (MPPT) units are used in a hybrid PV/FC system, one for the PV subsystem and the other one for the FC stack that significantly complicates the system implementation. In this study, a novel fast and highly accurate unified MPPT technique applicable to hybrid PV/FC systems is presented to address this problem. The technique uses a single algorithm to concurrently track the maximum power points (MPPs) of both PV module and FC stack. A hybrid PV/FC energy conversion system has been constructed, and it is experimentally verified that the novelties and contributions of this work are to present the only unified (PV/FC) MPPT technique reported in the literature having the highest MPPT efficiencies (99.60%, and 99.41%) along with the shortest convergence time (12 ms) compared to the state-of-the-art MPPT methods as demonstrated in Table 1, while the proposed unified MPPT method concurrently tracks two MPPs (PV module and FC stack) but the others track only one MPP. The rest of the paper is organized as follows. A concise survey about different MPPT methods applicable to PV and FC systems is presented in Section 2. Section 3 deals with the implementation of the proposed MPPT method in a hybrid PV/FC system. The performance of the MPPT method is evaluated in Section 4, and Section 5 concludes the paper.

2. MPPT methods applicable to PV and FC systems

In this section different MPPT methods used in PV and FC

E-mail address: h4477@hotmail.com.

http://dx.doi.org/10.1016/j.renene.2017.01.028
0960-1481/

Nomenclature

C_1	Parasitic capacitance of N-MOSFET switch
C_2	Converter's secondary-side serial capacitor
C_{in}	Converter's input capacitor
C_{out}	Converter's output capacitor
D_1 & D_2	Converter's diodes
D_S	Converter's duty cycle
D_{pv}	Duty cycle of the DC/DC converter connected to the PV module
D_{fc}	Duty cycle of the DC/DC converter connected to the FC stack
f_s	Converter's constant switching frequency
G	Solar irradiance
I_{pv}	PV module current
$I_{pv}(k)$	kth sample of the PV current
I_{fc}	FC stack current
$I_{fc}(k)$	kth sample of the FC stack current
L_{lk1}	Transformer's primary-side leakage inductor
L_{lk2}	Transformer's secondary-side leakage inductor
L_m	Transformer's equivalent magnetizing inductor
$n = N_2/N_1$	Transformer ratio
N_{cell}	Cells number of the FC stack
P_{pv}	PV module output power
$P_{pv}(k)$	kth sample of the PV output power
P_{pv-max}	PV output power at MPP
P_{fc}	FC stack output power
$P_{fc}(k)$	kth sample of the FC stack output power
P_{fc-max}	FC stack output power at MPP
S_1	Converter's N-MOSFET switch
t_{on}	Switch S_1 on-time.
T_s	Converter's switching period
T	PV cell temperature
V_{in}	Converter input voltage
V_{dc}	DC link voltage
V_{pv}	PV module voltage
V_{fc}	FC stack voltage
$V_{pv}(k)$	kth sample of the PV voltage
$V_{fc}(k)$	kth sample of the FC stack voltage
V_{pv-mpp}	PV voltage at MPP
V_{fc-mpp}	FC stack voltage at MPP
α_{pv}	PV power slope
α_{fc}	FC stack power slope
ΔD_{pv}	Step of duty cycle variation in the PV system
ΔD_{fc}	Step of duty cycle variation in the FC system

Table 1
Parameters of different MPPT methods and the proposed MPPT method in response to a solar irradiance step from 0 W m^{-2} to 1000 W m^{-2}.

MPPT method	Measured parameter(s)	Drawbacks & limitations	Convergence time (ms)	MPPT efficiency (%)	Data type
OCV [7]	Voltage	Offline, low accuracy	82	86	Simulation
Temperature method [8]	Voltage & Temperature	Offline, low accuracy	80	83	Simulation
SCC [9,10]	2 Currents	Offline, low accuracy, long convergence time	300	89	Simulation
Fuzzy logic [11,12]	Voltage & Current	Accuracy depends on selected roles	60	96	Simulation
Adaptive fuzzy [13]	Voltage & Current	Long convergence time	120	No report	Simulation
ANN [14]	Voltage & Current	Long convergence time & requiring training data	820	No report	Simulation
P&O fixed step-size [15]	Voltage & Current	Occurring oscillation, low accuracy	76	88	Simulation
P&O variable step-size [15]	Voltage & Current	Low accuracy	15	96	Simulation
Three-point weighted [16]	Voltage & Current	Low accuracy	47	96	Simulation
Dynamic P&O [17]	Voltage & Current	Long convergence time	1600	99.2	Simulation
Adaptive P&O [17]	Voltage & Current	Convergence time varies	≥30	98.76	Simulation
PSO-ANFIS [18]	Voltage & Current	Long convergence time	10000–17000	97–98	Simulation
P&O-ANFIS [18]	Voltage & Current	Long convergence time, low accuracy	12000–19000	85–97	Simulation
IC [19]	Voltage & Current	Occurring oscillation, low accuracy	81	95	Simulation
Variable step-size INR [20]	Voltage & Current	Long convergence time	≥ 150 ≥ 500	99.5 No report	Simulation Experimental
Modified IC [21]	Voltage & Current	Long convergence time	≥ 200	No report	Simulation
ESC [22–24]	Voltage & Current	Low accuracy	33	97	Simulation
Ripple-based ESC [25]	Voltage	Only applicable to grid-connected PV, long convergence time	520	99.69–99.85	Simulation
PM-MPPT [26]	Voltage & Current	Complicated structure	Not reported	99.2	Simulation
Scanning technique [27]	Voltage & Current	Long convergence time	2000	No report	Experimental
MPPT with irradiance sensor [28]	Voltage & Current & irradiance	Long convergence time & requiring irradiance sensors	Not reported	98.62	Simulation
Hybrid prediction-P&O [29]	Voltage & Current	Long convergence time	≥3000	No report	Experimental
Cuckoo Search (CS) [30]	Voltage & Current	–	100–250	No report	Simulation
FPGA [31]	Voltage & Current	–	≥25	No report	Simulation
Auto-scaling variable step-size IC [32]	Voltage & Current	Large number of calculations, long convergence time	≥520	No report	Simulation
GA [33]	Voltage & Current	MPPT efficiency varies, long convergence time	≥600	96–99	Simulation
Predictive [34]	Voltage & Current	Low accuracy, long convergence time	245	95.8	Simulation
This work	**Voltage & Current**	–	**12**	**≥99.60**	**Experimental results**

systems are introduced in two distinct sub-sections, and advantages and drawbacks of each method are explained in detail.

2.1. MPPT methods applicable to PV systems

A MPPT controller tracks the MPP of a PV module/panel, and so

enhances the energy efficiency [5,6]. Different MPPT techniques have been reported in the literature that are explained in detail. Open-circuit voltage (OCV) method first measures the open-circuit voltage of the PV module disconnected from the system, and then estimates the voltage associated with the MPP [7]. When environmental conditions such as ambient temperature vary over time, the PV module should be regularly disconnected from the system (offline operation) to measure the open-circuit voltage, so the technique is a low-accuracy offline method as reported in Table 1. Temperature method is a modified version of the OCV method that estimates the open-circuit voltage from the PV cell temperature based on the consumption that the open-circuit voltage is proportional to the cell temperature [8], and so the same drawbacks exist. Similar to the OCV method, short-circuit current (SCC) technique is a low-accuracy offline method which uses the short-circuit current of a PV module instead of the open-circuit voltage to estimate its MPP [9,10]. Fuzzy methods convert the voltage and current of a PV module into fuzzy variables, and then, some selected fuzzy roles are used to track MPP, because of the uncertainty available in fuzzy roles, the accuracy level is low, and significantly varies with change in the selected roles [11,12]. Adaptive fuzzy MPPT method [13] is a modified version in which a fuzzy controller with an adaptive gain is used to improve the accuracy, although the convergence time becomes longer. An artificial neural network (ANN) MPPT method uses a neural network trained by real data comprising the voltage and current associated with MPP under different condition [14]. Long convergence time and requiring training data that explicitly complicates the system implementation are the main disadvantages as reported in Table 1. Perturb and observe (P&O) technique uses the voltage and current perturbations to find MPP. Fixed step-size P&O [15], variable step-size P&O [15] and three-point weighted P&O [16] are the three classic versions of this technique. There are also three modified versions called “adaptive P&O”, “dynamic P&O”, and “P&O adaptive neuro-fuzzy inference system (P&O-ANFIS)”. Comparing the dynamic P&O method, which applies a dynamic perturbation step-size to reduce oscillations, to the adaptive P&O method demonstrated higher MPPT efficiency of the dynamic type [17]. Comparing the P&O-ANFIS MPPT algorithm to a particle swarm optimization ANFIS (PSO-ANFIS) algorithm showed that PSO-ANFIS MPPT method exceeds in performance [18]. The drawbacks of each version of the P&O method are summarized in Table 1, occurring oscillations, long convergence time and low accuracy are the main drawbacks. The *P-V* curve slope is used to track MPP in incremental conductance (IC) method [19], two improved versions of the IC technique called “variable step-size incremental resistance (INR)” [20] and “modified IC” [21] are also available in which oscillations around MPP have been reduced. Similar to the previous method the disadvantages are occurring oscillation (in the main version), long convergence time, and low accuracy. Extremum seeking control (ESC) MPPT method applies a nonlinear feedback to adapt the operating point of a system with that of the PV module used in the system, and then estimates MPP [22–24]. Ripple-based ESC method is a modified version only applicable to grid-connected PV systems that utilizes DC-link voltage ripple as a merging signal to find MPP [25]. In practice, the harmonics resulted from harmonically distorted and unbalanced grid voltages make it impossible to high accurately extract voltage ripple, and hence, the MPPT efficiency significantly decreases. A cell-level distributed MPPT structure is used in power management (PM) MPPT method, so that, an independent MPPT circuit is dedicated to each PV cell, and so each cell produces its own maximum power. The method has a complicated and expensive architecture, and is more suitable for shaded situations [26]. Scanning method finds MPP by scanning and comparing output powers obtained during MPPT process [27], the convergence speed is low, and so the convergence time is long as reported in Table 1. A sensor based MPPT method first measures solar irradiance using some photodiodes, and then, based on the irradiance level, determines which algorithm should be executed [28]. The method needs irradiance sensors, and moreover, MPPT process is performed in several steps that makes longer the convergence time. Prediction-P&O method is a hybrid method that combines the direct-prediction technique with the P&O method [29], many calculations should be performed, and so the convergence time is long. Cuckoo search (CS) MPPT method uses the CS algorithm which provides several advantages such as fast convergence, higher efficiency, and utilizing fewer tuning parameters [30]. Field program gate array (FPGA) MPPT method finds MPP by comparing instant output power with maximum power obtained theoretically to estimate maximum power and related voltage level [31]. Auto-scaling variable step-size IC MPPT method uses a judgment criterion and auto-scaling variable step-size to enable the PV system to achieve a fast dynamic response and stable output power [32], although the convergence time is not short because a large number of calculations should be performed. Genetic algorithm (GA) MPPT method applies the GA, the convergence speed is low, and moreover, the MPPT efficiency varies with reiterating the experiment [33]. Predictive MPPT method utilizes a model predictive controller to track MPP, the method exhibits a good performance under partially shaded conditions, although the accuracy and convergence speed are low [34]. Some of the above-mentioned methods such as P&O technique are also applicable to other systems such as wind energy conversion systems [35]. In a PV system, in addition to maximum power extraction, the MPPT controller can be also used to control other devices such as a solar tracker [36,37].

2.2. MPPT methods applicable to FC systems

FC stacks are efficient electrochemical power sources with low pollution in which electrical power is produced by way of the chemical reaction between oxygen and hydrogen [38]. The MPPT methods used in FC based power generation systems are some of the same MPPT methods used in PV systems that were explained in detail. The MPPT method reported in Ref. [39] regulates load resistance to track the MPP of a microbial fuel cell, while the MPPT technique proposed in Ref. [40] continually detects the MPP of a FC, and then, varies the load to match it with the MPP. Similar to what explained in detail for PV systems, the fuzzy, P&O, ANN, and ESC MPPT methods are applicable to FC systems [41–44]. Varying output impedance to track MPP is another technique [45]. Utilizing potentiometers to maximize output power, and adjusting the voltage of a microbial FC to one third of the open-circuit voltage are the two other methods having very low accuracy [46,47].

3. Implementation of the proposed MPPT method in a hybrid PV/FC system

In this section, the implementation of the proposed unified MPPT technique is analyzed in detail. The configuration of the hybrid PV/FC energy conversion system in which the proposed MPPT technique has been implemented as a MPPT unit is shown in Fig. 1. In fact, it is an energy conversion system comprising two subsystems (PV and FC) combined to each other to produce electric power [48]. As shown in Fig. 1, each subsystem is connected to the DC bus through a dedicated DC/DC boost converter, and the MPPT unit simultaneously tracks the maximum power points of the two subsystems using the DC link voltage as a reference voltage. The circuit of the DC/DC converter used in the PV and FC subsystems is shown in Fig. 2 [49]. It is a high-efficient DC/DC boost converter including only one N-MOSFET switch S_1. The switch S_1 operates

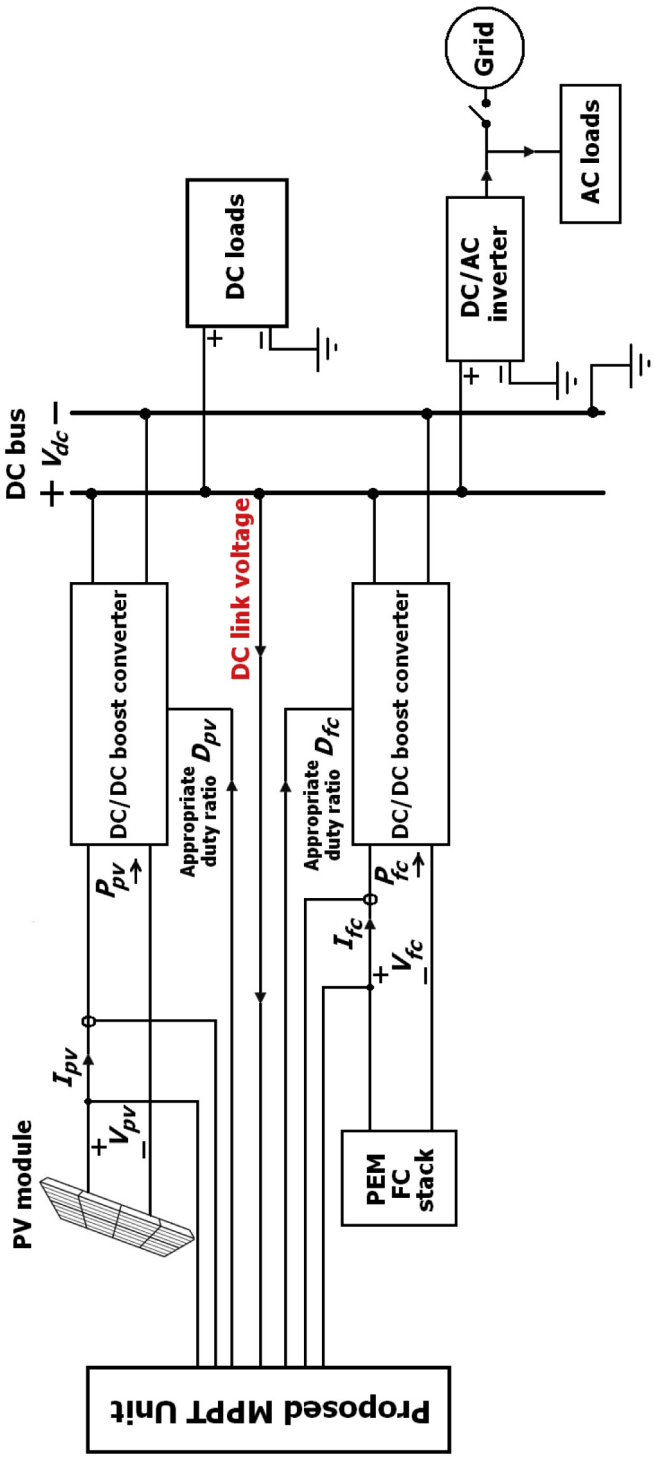

Fig. 1. Configuration of the hybrid PV/FC energy conversion system including the proposed unified MPPT unit.

with a constant switching frequency (f_s) and variable duty cycle (D_S). The gain of the converter is given as [49]:

$$\frac{V_{dc}}{V_{in}} = \frac{n}{1 - D_S} \tag{1}$$

As shown in Fig. 1, V_{dc} is the converter output voltage which is the DC link voltage occurring on the DC bus.

3.1. PV subsystem

In this sub-section, the PV subsection of the hybrid PV/FC energy conversion system is analyzed in detail. The output power of the PV module shown in Fig. 1 is obtained as:

$$P_{pv} = V_{pv}\, I_{pv} \tag{2}$$

The *P-V* characteristic of a typical PV module is shown in Fig. 3, where the *P-V* curve has been divided into three parts: the MPP, the left side of the MPP, and the right side of the MPP. At the MPP, the PV power derivative is zero, so:

$$\frac{dP_{pv}}{dV_{pv}} = 0 \tag{3}$$

At the left side of the MPP, the derivative is positive, so:

$$\frac{dP_{pv}}{dV_{pv}} > 0 \tag{4}$$

Similarly, at the right side, it is negative, so:

$$\frac{dP_{pv}}{dV_{pv}} < 0 \tag{5}$$

The PV power derivative is approximated by defining power slope α_{pv} as:

$$\frac{dP_{pv}}{dV_{pv}} \approx \frac{\Delta P_{pv}}{\Delta V_{pv}} = \frac{P_{pv}(k) - P_{pv}(k-1)}{V_{pv}(k) - V_{pv}(k-1)} = \alpha_{pv} \tag{6}$$

$P_{pv}(k)$ is computed as:

$$P_{pv}(k) = V_{pv}(k) I_{pv}(k) \tag{7}$$

The relationship between the DC link voltage of the hybrid PV/FC system and the PV voltage can be expressed using Eq. (1) as:

$$V_{pv} = \frac{(1 - D_{pv})\, V_{dc}}{n} \tag{8}$$

Since the DC link voltage is constant, the PV voltage V_{pv} can be regulated to the PV voltage at the MPP (V_{pv-mpp}) by varying the duty cycle D_{pv}, so that, V_{pv} is increased by deceasing D_{pv}, and is decreased by increasing D_{pv}. Thus, MPPT can be performed by varying the duty cycle D_{pv}. The flowchart of the proposed MPPT algorithm implemented in the PV subsystem is shown in Fig. 4. The PV voltage $V_{pv}(k)$ and current $I_{pv}(k)$ are continually measured, and the PV output power $P_{pv}(k)$ is computed using Eq. (7) by the MPPT unit, then the power slope α_{pv} is calculated using Eq. (6). If $\alpha_{pv} = 0$ (at the MPP), there is no need to change D_{pv}. If $\alpha_{pv} > 0$ (the left side of the MPP), V_{pv} is continually increased by decreasing D_{pv}, i.e., $D_{pv}(k+1) = D_{pv}(k) - \Delta D_{pv}$, where ΔD_{pv} is a positive amount that will be explained next. If $\alpha_{pv} < 0$ (the right side of the MPP), V_{pv} is continually decreased by increasingD_{pv}, i.e., $D_{pv}(k+1) = D_{pv}(k) + \Delta D_{pv}$, until the operating point of the PV module reaches the MPP. When $\Delta V_{pv} = 0$, the MPPT unit waits for the next sample of the PV module voltage as shown in the flowchart. As mentioned, the increase/decrease in D_{pv} is performed by adding/subtracting the positive amount ΔD_{pv} to/from D_{pv}. In this study, more than 50 experiments were performed for the constructed PV subsystem under different conditions (different solar irradiances and temperatures) that demonstrated choosing ΔD_{pv} according to the following equation provides not only a minimal tracking convergence time but also a maximal MPPT efficiency:

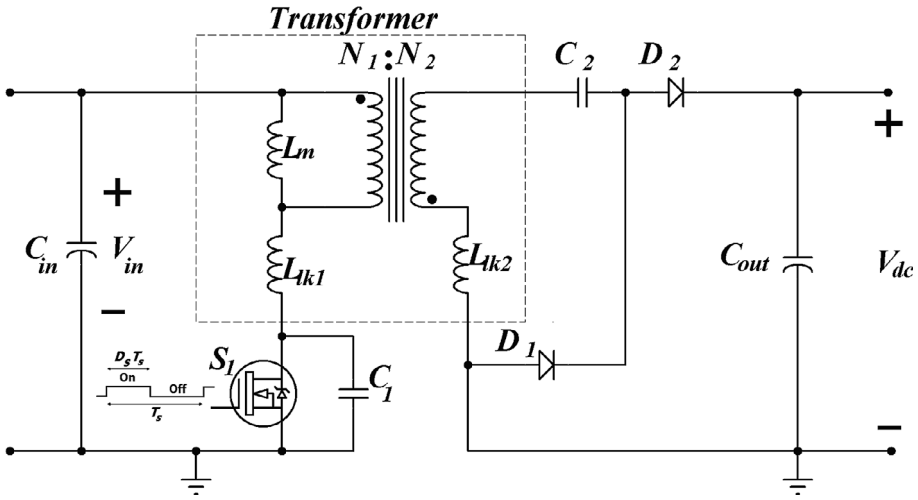

Fig. 2. DC/DC boost converter used in the PV and FC subsystems.

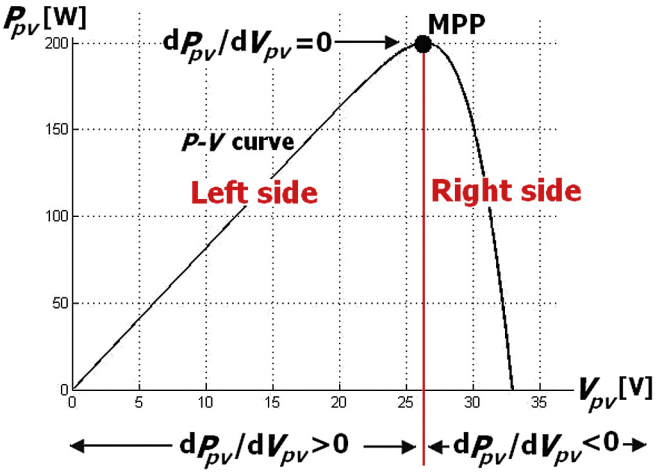

Fig. 3. *P-V* characteristic of a typical PV module.

$$\Delta D_{pv} = \begin{cases} 0.100 & \text{when } |\alpha_{pv}| \geq 2 \text{ W V}^{-1} \\ 0.050 & \text{when } 0.5 \text{ W V}^{-1} \leq |\alpha_{pv}| < 2 \text{ W V}^{-1} \\ 0.010 & \text{when } 0.1 \text{ W V}^{-1} \leq |\alpha_{pv}| < 0.5 \text{ W V}^{-1} \\ 0.005 & \text{when } 0.05 \text{ W V}^{-1} \leq |\alpha_{pv}| < 0.1 \text{ W V}^{-1} \\ 0.001 & \text{when } 0 \text{ W V}^{-1} \leq |\alpha_{pv}| < 0.05 \text{ W V}^{-1} \end{cases} \quad (9)$$

Noting Eq. (9) shows that, when the MPP is far from the PV operating point, $|\alpha_{pv}|$ is high, so to significantly decrease the tracking convergence time, ΔD_{pv} is selected larger. This selection significantly decreases the amount of time it takes to move the operating point to around the MPP, and so minimizes the tracking convergence time. By reduction in the distance between the operating point and the MPP, $|\alpha_{pv}|$ becomes lower and lower, and so ΔD_{pv} is chosen smaller and smaller to maximize the MPPT efficiency (accuracy of the MPPT process).

3.2. FC subsystem

In this sub-section, the FC subsection of the hybrid PV/FC energy conversion system is explained and analyzed in detail. The output power of the FC stack shown in Fig. 1 is obtained as:

$$P_{fc} = V_{fc} I_{fc} \quad (10)$$

The *P-V* characteristic of a typical FC stack is shown in Fig. 5. The *P-V* curve has been divided into the three parts: the MPP where $\frac{dP_{fc}}{dV_{fc}} = 0$, the left side of the MPP where $\frac{dP_{fc}}{dV_{fc}} > 0$, and the right side of the MPP where $\frac{dP_{fc}}{dV_{fc}} < 0$. Similar to the PV subsystem, the derivative of the FC stack power is approximated by defining power slope α_{fc} as:

$$\frac{dP_{fc}}{dV_{fc}} \approx \frac{\Delta P_{fc}}{\Delta V_{fc}} = \frac{P_{fc}(k) - P_{fc}(k-1)}{V_{fc}(k) - V_{fc}(k-1)} = \alpha_{fc} \quad (11)$$

$P_{fc}(k)$ is computed as:

$$P_{fc}(k) = V_{fc}(k) I_{fc}(k) \quad (12)$$

The relationship between the DC link voltage, which is a constant voltage, and the FC stack voltage is obtained using Eq. (1) as:

$$V_{fc} = \frac{\left(1 - D_{fc}\right) V_{dc}}{n} \quad (13)$$

where D_{fc} is the duty cycle of the DC/DC boost converter dedicated to the FC stack. Comparing Eqs. (11)–(13) to Eqs. (6)–(8) shows that the MPPT technique used for the PV subsystem can be also utilized to track the MPP of the FC stack. Thus, similar to the PV subsystem, the proposed MPPT method varies the duty cycle D_{fc} to regulate the stack voltage to the stack voltage at the MPP (V_{fc-mpp}) as shown in Fig. 4. The increase/decrease in D_{fc} is performed by adding/subtracting a positive amount ΔD_{fc} to/from D_{fc}. Similar to the PV subsystem, more than 50 experiments were performed for the constructed FC subsystem under different conditions (different ambient pressures and temperatures) that demonstrated choosing ΔD_{fc} according to the following equation provides a minimal tracking convergence along with a maximal MPPT efficiency:

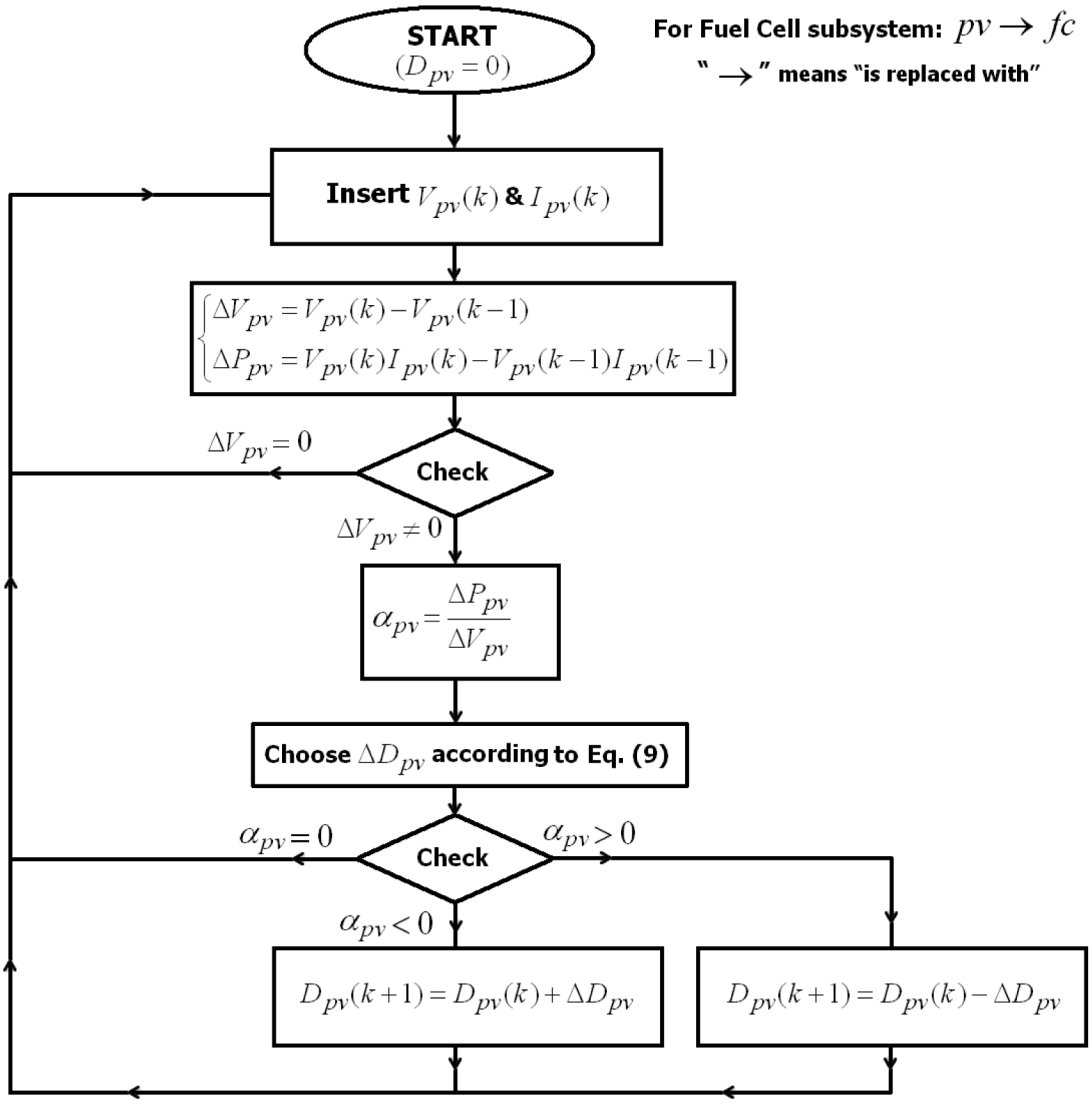

Fig. 4. Flowchart of the MPPT process in the PV and FC subsystems performed by the unified MPPT unit.

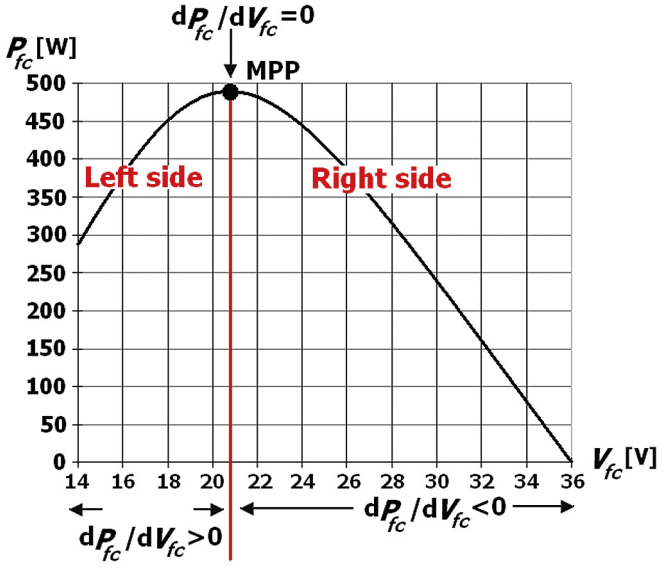

Fig. 5. *P-V* characteristic of a typical FC stack.

$$\Delta D_{fc}=\begin{cases}0.100 & \text{when } \left|\alpha_{fc}\right|\geq 15\ \text{W V}^{-1}\\ 0.050 & \text{when } 5\ \text{W V}^{-1}\leq\left|\alpha_{fc}\right|<15\ \text{W V}^{-1}\\ 0.010 & \text{when } 1\ \text{W V}^{-1}\leq\left|\alpha_{fc}\right|<5\ \text{W V}^{-1}\\ 0.005 & \text{when } 0.5\ \text{W V}^{-1}\leq\left|\alpha_{fc}\right|<1\ \text{W V}^{-1}\\ 0.001 & \text{when } 0\ \text{W V}^{-1}\leq\left|\alpha_{fc}\right|<0.5\ \text{W V}^{-1}\end{cases} \quad (14)$$

4. Experimental results and performance evaluation

In this section, experimental verifications obtained from different experiments performed by using the constructed hybrid PV/FC system are presented. Based on the hybrid PV/FC system the configuration of which is shown in Fig. 1, a hybrid PV/FC power generation system has been built to evaluate the performance of the proposed MPPT technique. The electric circuit of the constructed hybrid PV/FC power system is shown in Fig. 6. A microcontroller MC68HC11E9 has been used to implement the MPPT unit. The flowchart shown in Fig. 4 has been utilized to program the

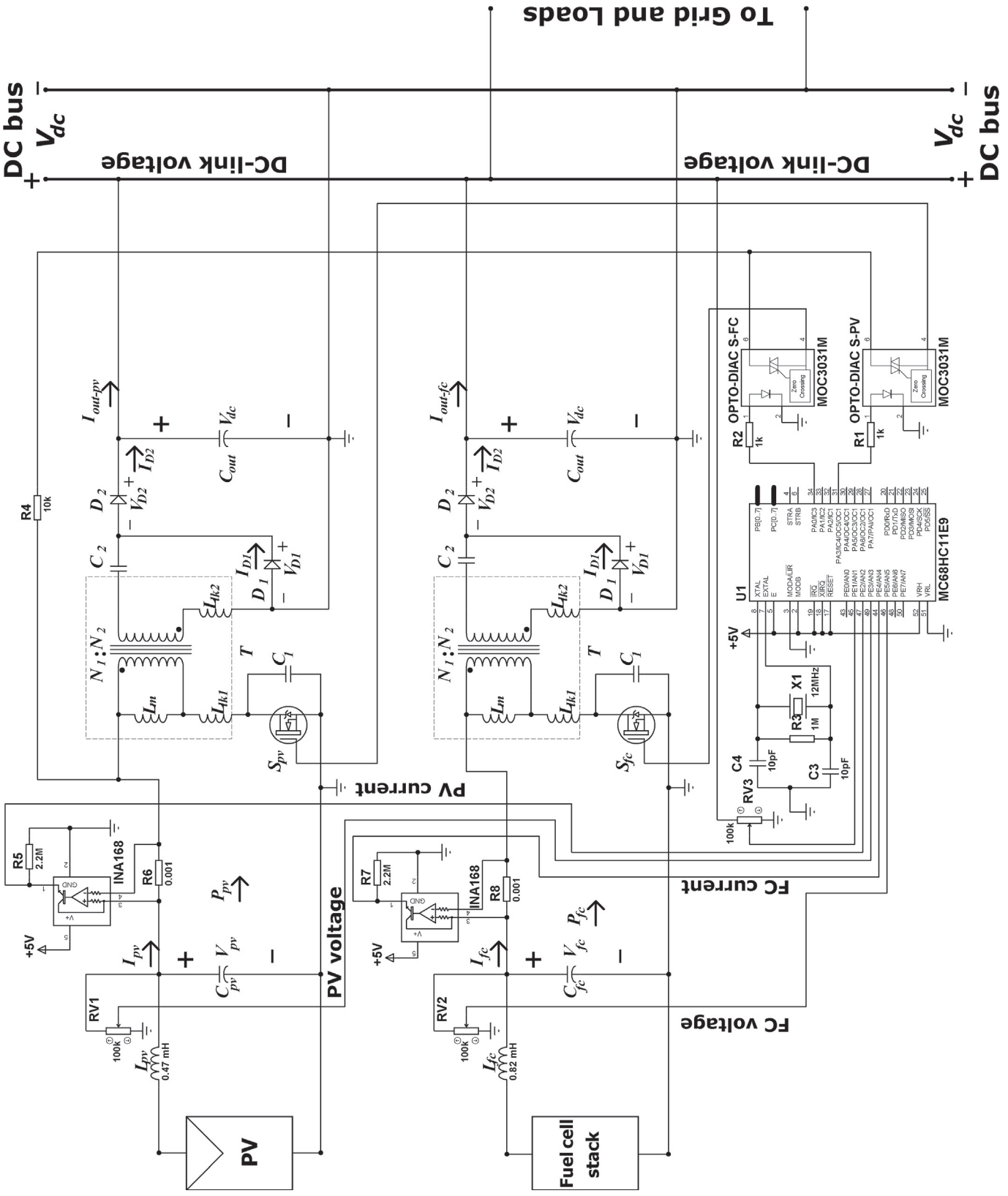

Fig. 6. Electric circuit of the constructed hybrid PV/FC power generation system including the proposed unified MPPT controller.

microcontroller to find the maximum power points of the PV and FC subsystems. In each subsystem, the converter input current is continually measured by INA 168, and is supplied to the microcontroller through an analog/digital (A/D) pin. The converter input voltage is first scaled by a potentiometer (RV1 and RV2), and then, is supplied to an A/D pin of the microcontroller. The

microcontroller continually samples the currents and voltages of the PV module and FC stack with a sampling period of 100 μs, and the suitable duty ratios D_{pv} and D_{fc} are produced by the microcontroller according to the flowchart of the MPPT process shown in Fig. 4. Then, the duty ratios D_{pv} and D_{fc} are supplied to the MOSFET switches S_{pv} and S_{fc} through the two opto-diacs S-PV and S-FC as two periodic switching pulses with the duty cycles of D_{pv} and D_{fc}. Switching S_{pv} and S_{fc} with the duty cycles of respectively D_{pv} and D_{fc} regulates the input powers of the two DC/DC boost converters (P_{pv} and P_{fc}) to their maximum values (P_{pv-max} and P_{fc-max}) by varying the input voltages of the two converters (V_{pv} and V_{fc}). All parts of the constructed hybrid PV/FC power generation system are original (unified MPPT controller, FC subsystem, PV subsystem, couplers, DC bus, etc) except the DC/DC converter that has been taken from Ref. [49]. It is clear that the MPPT method is also applicable to an only PV or FC system. When the method is applied to a PV system, the voltage and current of the FC stack are disconnected from the MPPT controller, and similarly, when it is applied to a FC system, the voltage and current of the PV module are disconnected. It is also reminded that when the constructed hybrid system is connected to the local power distribution network [50], an extra protection circuit is also needed against the different faults that occur in the grid such as ground, phase to phase and short-circuit faults [51,52]. The parameters and specifications of the components used in the constructed hybrid PV/FC power generation system are summarized in Tables 2–4. To evaluate the performance of the method, the MPPT process in each subsystem has been evaluated separately by performing different experiments that are explained in detail in two sub-sections as follows.

4.1. Experimental results related to the PV subsystem

As reported in Table 3, a PV module KC200GT has been used in the constructed hybrid power system that its experimental *P-V* characteristics obtained under nominal condition (solar irradiance $G = 1000$ W m^{-2}, cell temperature $T = 25$ C∘) and nominal condition with different shading effects (different solar irradiance levels) are shown in Fig. 7. To obtain the static-dynamic response of the proposed MPPT technique which is the key parameter representing not only the accuracy of the MPPT process but also the MPPT efficiency, four 20% filmy glasses have been utilized to provide uniform irradiance and non-uniform irradiance (partially shaded) situations. The four 20% filmy glasses were first put on the PV module, each 20% filmy glass causes a 20% shading effect, so a shadow with 80% shading effect occurred, and the solar irradiance on the PV module became 200 W m^{-2}. After 60 s, the first filmy glass was uniformly taken out from the left side of the module during 5 s. This process was repeated for the other three filmy glasses, so the solar irradiance absorbed by the PV module increased 200 W m^{-2} by 200 W m^{-2} after each one minute, and

Table 2
Parameters s of the two DC/DC boost converters used in the hybrid PV/FC energy conversion system.

C_{in} (μ F)-Aluminum electrolytic capacitor/100 V	680
Converter switching frequency: f_s (kHz)	100
C_{out} (μ F)-Aluminum electrolytic capacitor/250 V	220
DC-link voltage: V_{dc} (V)	310
C_2 (μ F)-Premium metallized polypropylene capacitor/400 V	18
C_1 (n F)-Parasitic capacitance of MOSFET IRF1407	1.2
Type of transformer	Pulse
10/4	$n = N_2/N_1$
L_m (μ H)	19.14
L_{lk2} (μ H)	0.031
L_{lk1} (μ H)	0.011
MOSFET switch S_1	IRF1407
Equivalent series resistance of C_{out} at 10 kHz: (mΩ)	478
Diodes D_1 and D_2	15ETH06S

Table 3
Parameters of the PV module KC200GT used in the hybrid PV/FC energy conversion system.

Current at MPP: I_{pv-mpp} (A)	7.61
Voltage at MPP: V_{pv-mpp} (V)	26.3
Output power at MPP: P_{pv-mpp} (W)	200.1430
Short-circuit current: I_{SC} (A)	8.21
Open-circuit voltage: V_{OC} (V)	32.9

Table 4
Parameters and specifications of the FC stack used in the hybrid PV/FC energy conversion system.

Model	Horizon H-1000 PEM
Cells number (N_{cell})	48
Stack efficiency	40% @ 28.8 V
Rated power (W)	1000
Operating point	28.8 V @ 35 A
Maximum stack temperature (°C)	65
Over current shut down (A)	42
Low voltage shut down (V)	24

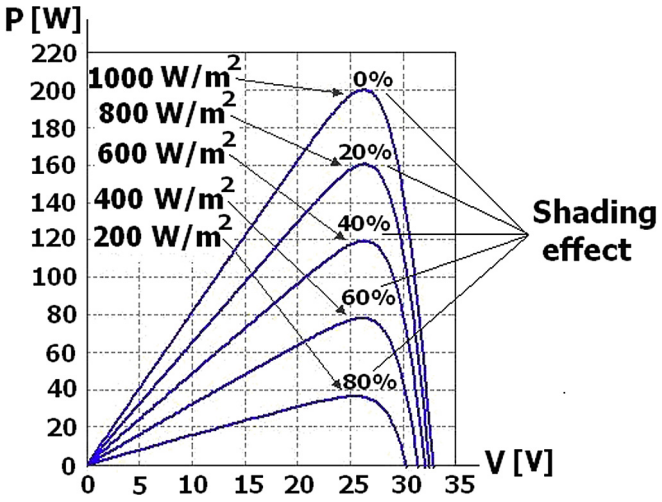

Fig. 7. Experimental *P-V* curves of PV module KC200GT, $T = 25$ °C.

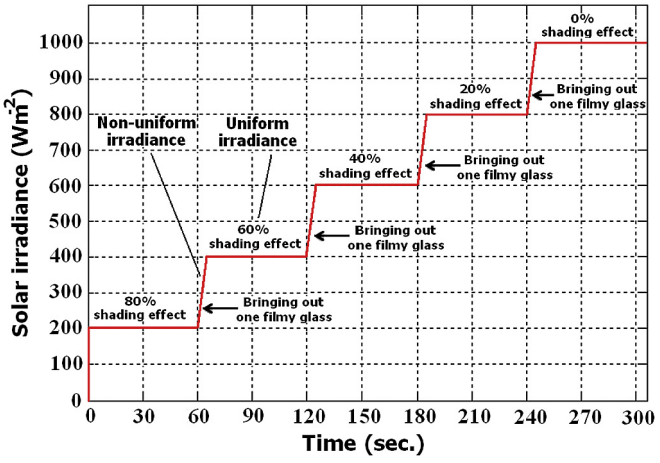

Fig. 8. Pattern of the solar irradiance variation ($T = 25$°C).

uniform and non-uniform irradiance conditions occurred as shown in Fig. 8. The experimental waveform of the PV output power (P_{pv}) extracted by the MPPT controller showing the static-dynamic response of the proposed MPPT technique obtained under the mentioned uniform irradiance and partially shaded conditions is shown in Fig. 9. Noting the static-dynamic response, and considering the solar irradiance pattern shown in Fig. 8 and the maximum available powers associated with the different levels of solar irradiance shown in Fig. 7 explicitly verifies that the MPPT controller performs a highly accurate and fast MPPT in the PV subsystem. For instance, on the one hand, the static-dynamic response indicates that the PV output powers extracted by the MPPT controller under nominal condition (G_n = 1000 W m^{-2}), and under nominal condition with 20% shading effect (G = 800 W m^{-2}) are 199.28 W and 160.11 W, respectively. On the other hand, the maximum available powers of the PV module associated with the irradiances of 1000 W m^{-2} and 800 W m^{-2} are respectively 200.08 W and 160.69 W as shown in Fig. 7. Thus, the MPPT efficiency of the proposed MPPT method under nominal condition is obtained as:

$$\text{MPPT efficiency} = \frac{199.28}{200.08} \times 100 = 99.60\% \quad (15)$$

Similarly, the MPPT efficiency under nominal condition with 20% shading effect is found as:

$$\text{MPPT efficiency} = \frac{160.11}{160.69} \times 100 = 99.64\% \quad (16)$$

Noting Eqs. (15) and (16) shows that the MPPT efficiency of the tracker is more than 99.60%, and this experimentally verifies that the MPPT performed by the MPPT method is a highly accurate tracking process. The experimental waveform indicating the response of the MPPT controller to a positive solar irradiance step from 0 W m^{-2} to 1000 W m^{-2} obtained under nominal condition is also shown Fig. 10. The time response not only explicitly demonstrates the very fast response of the MPPT controller to the sudden variation in solar irradiance, so that, the tracking convergence time is only 12 ms but also again verifies that the proposed MPPT technique has a very high MPPT efficiency of more than 99.60% under nominal condition. To highlight the excellent performance of the proposed method, a comparison between its parameters and the state-of-the-art MPPT methods is performed in Table 1. The comparison explicitly verifies that the MPPT method presented in this work has the shortest convergence time (12 ms) along with the highest MPPT efficiency (99.6%) compared to the state-of-the-art MPPT methods, while the proposed MPPT method concurrently tracks two maximum power points (PV module and FC stack) but the others track only one MPP.

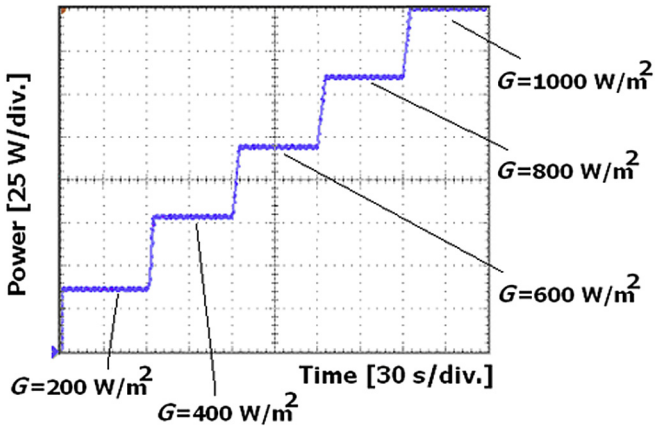

Fig. 9. Experimental waveform of the PV output power extracted by the MPPT controller.

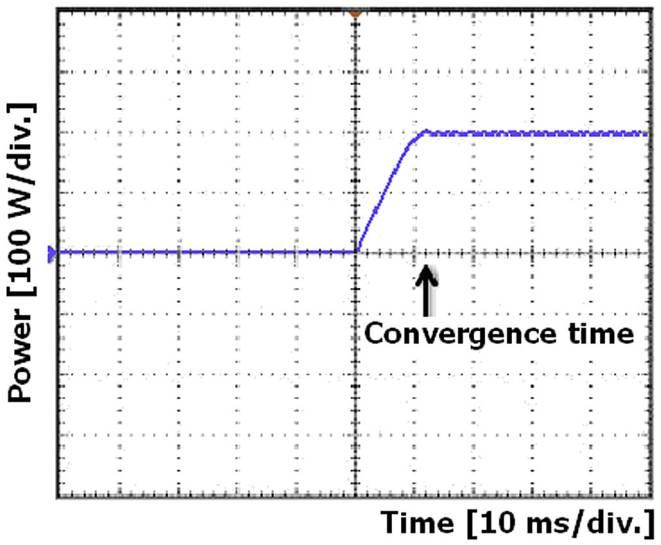

Fig. 10. Response of the MPPT technique presented in this study to a positive solar irradiance step from 0 W m^{-2} to 1000 W m^{-2}.

4.2. Experimental results related to the FC subsystem

As reported in Table 4, one H-1000 proton exchange membrane (PEM) FC stack has been used in the constructed hybrid power generation system. The stack itself has a control unit that regulates the flow rate of the hydrogen consumed by the stack. The experimental *P-V* characteristic of the H-1000 PEM FC stack obtained at ambient pressure and temperature of respectively 0.996 atm and 27 °C is shown in Fig. 11 that is compatible with the experimental results provided in the user manual of the H-1000 PEM FC stack [53] and the technical specifications reported in Table 4. As shown in Fig. 11, and reported in Table 4 and the user manual, the maximum output power of the stack is 1000 W associated with the MPP (28.8 V, 1000 W).

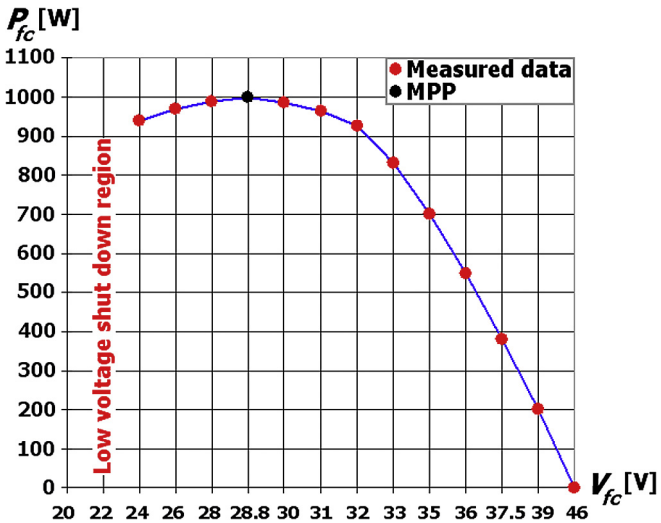

Fig. 11. Experimental *P-V* characteristic of the H-1000 PEM FC stack obtained at ambient pressure and temperature of respectively 0.996 atm and 27 °C.

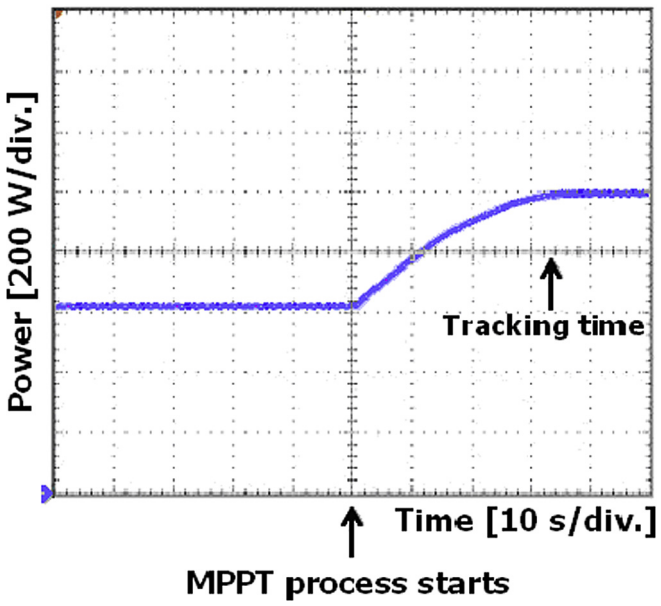

Fig. 12. Experimental waveform of the output power of the H-1000 PEM FC stack extracted by the MPPT controller.

To evaluate the performance of the MPPT technique to track the MPP of the FC stack, the FC stack was turned on, while the MPPT controller was not active, the output power of the stack (P_{fc}) reached about 620 W, and then, the MPPT controller was suddenly turned on at $t = 0$ as shown in Fig. 12. The experimental waveform of the stack output power extracted by the MPPT controller is shown in Fig. 12 that demonstrates the tracking convergence time is about 33 s which is a very short time for a PEM FC stack with the rated power of 1000 W in which very slow chemical reactions cause a considerable time delay in the MPPT process. Moreover, the power waveform shows that the average output power of the H-1000 PEM FC stack extracted by the MPPT controller is 994.12 W. Now, by comparing this amount with the available maximum output power of the stack reported in the user manual [53], Table 4, and shown in Fig. 11, the MPPT efficiency of the MPPT method can be computed as:

$$\text{MPPT efficiency} = \frac{994.12}{1000} \times 100 = 99.41\% \tag{17}$$

Thus, similar to the PV subsystem, the proposed MPPT method performs a very fast and highly accurate MPPT process with the MPPT efficiency of more than 99.41% and a very short convergence time of at most 33 s in the FC subsystem. The photos of the experimental set-up consisting of the constructed system, PV module, and FC stack are shown in Fig. 13 (a)-(c).

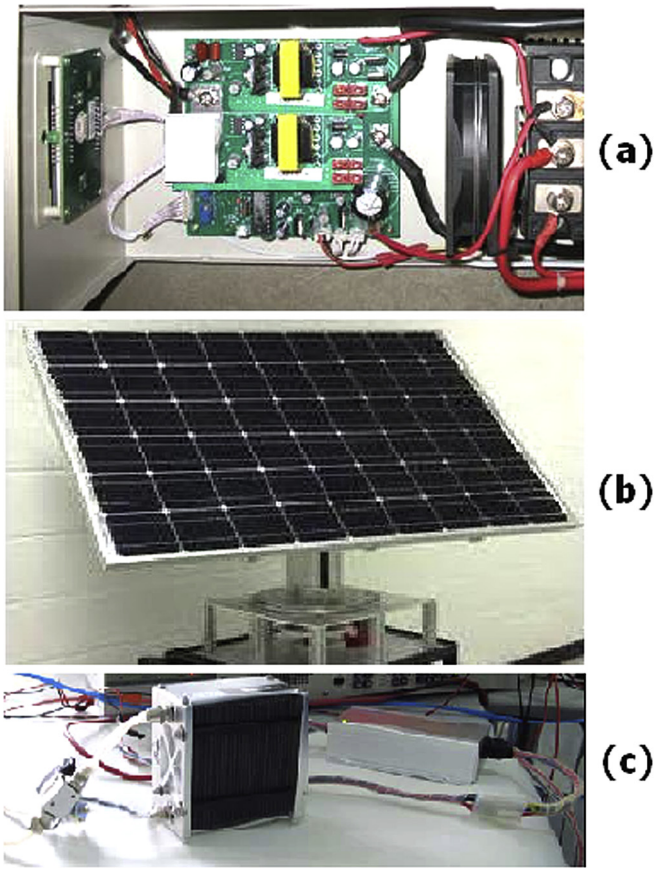

Fig. 13. Experimental set-up: (a) Constructed system. (b) PV module. (c) FC stack.

5. Conclusion

Two MPPT units are currently used in hybrid PV/FC systems, one for the PV subsystem and the other one for the FC stack, which significantly increases the system cost and complication. This study addressed this problem by presenting a novel fast and highly accurate unified MPPT technique that is the only unified MPPT technique reported in the literature. It was shown that the method only uses the output voltages and currents of the PV module and FC stack used in a hybrid PV/FC system to concurrently track the MPPs of both PV module and FC stack. A hybrid PV/FC power generation system was constructed, and the excellent performance of the unified MPPT method was experimentally verified, so that, the MPPT efficiency in the PV and FC subsystems was measured as 99.60% and 99.41%, respectively, along with the convergence time of respectively 12 ms and 33 s. The method was compared to the state-of-the-art MPPT methods that demonstrated it provides the highest MPPT efficiencies along with the shortest convergence time. Furthermore, the MPPT technique presented in this study is applicable to both standalone and grid-connected versions of PV, FC and hybrid PV/FC systems.

References

[1] H. Fathabadi, Novel solar powered electric vehicle charging station with the capability of vehicle-to-grid, Solar Energy 142 (2017) 136–143, http://dx.doi.org/10.1016/j.solener.2016.11.037.
[2] H. Fathabadi, Novel wind powered electric vehicle charging station with vehicle-to-grid (V2G) connection capability, Energy Conversion and Management 136 (2017) 229–239, http://dx.doi.org/10.1016/j.enconman.2016.12.045.
[3] H. Fathabadi, Utilization of electric vehicles and renewable energy sources used as distributed generators for improving characteristics of electric power distribution systems, Energy 90 (2015) 1100–1110.
[4] N. Mezzai, D. Rekioua, T. Rekioua, A. Mohammedi, K. Idjdarane, S. Bacha, Modeling of hybrid photovoltaic/wind/fuel cells power system, Int. J. Hydrogen Energy 39 (27) (2014) 15158–15168.
[5] H. Fathabadi, Lambert *W* function-based technique for tracking the maximum power point of PV modules connected in various configurations, Renew. Energy 74 (2015) 214–226.
[6] H. Fathabadi, Novel photovoltaic based battery charger including novel high efficiency step-up DC/DC converter and novel high accurate fast maximum power point tracking controller, Energy Convers. Manag. 110 (2016) 200–211.
[7] J.H.R. Enslin, M.S. Wolf, D.B. Snyman, W. Swiegers, Integrated photovoltaic maximum power point tracking converter, IEEE Trans. Ind. Electron. 44 (1997) 769–773.
[8] M. Park, In-Keun Yu, A study on the optimal voltage for MPPT obtained by surface temperature of solar cell, in: 30th Annual Conference of IEEE 3, 2004,

pp. 2040–2045.
[9] M.A.S. Masoum, H. Dehbonei, E.F. Fuchs, Theoretical and experimental analyses of photovoltaic systems with voltage and current-based maximum power-point tracking, IEEE Trans. Energy Convers. 17 (4) (2002) 514–522.
[10] T. Noguchi, S. Togashi, R. Nakamoto, Short-current pulse-based maximum-power-point tracking method for multiple photovoltaic-and-converter module system, IEEE Trans. Ind. Electron. 49 (1) (2002) 217–223.
[11] C.B. Salah, M. Ouali, Comparison of fuzzy logic and neural network in maximum power point tracker for PV systems, Electr. Power Syst. Res. 81 (2011) 43–50.
[12] M.M. Algazar, H. AL-monier, H.A. EL-halim, M.E. El Kotb Salem, Maximum power point tracking using fuzzy logic control, Int. J. Electr. Power Energy Syst. 39 (1) (2012) 21–28.
[13] O. Guenounou, B. Dahhou, F. Chabour, Adaptive fuzzy controller based MPPT for photovoltaic systems, Energy Convers. Manag. 78 (2014) 843–850.
[14] S.A. Rizzo, G. Scelba, ANN based MPPT method for rapidly variable shading conditions, Appl. Energy 145 (2015) 124–132.
[15] A.K. Abdelsalam, A.M. Massoud, S. Ahmed, P.N. Enjeti, High-performance adaptive perturb and observe MPPT technique for photovoltaic-based microgrids, IEEE Trans. Power Electron. 26 (4) (2011) 1010–1021.
[16] J.A. Jiang, T.L. Huang, Y.T. Hsiao, C.H. Chen, Maximum power tracking for photovoltaic power systems, J. Sci. Eng. 8 (2) (2005) 147–153.
[17] J. Ahmed, Z. Salam, An improved perturb and observe (P&O) maximum power point tracking (MPPT) algorithm for higher efficiency, Appl. Energy 150 (2015) 97–108.
[18] M. Muthuramalingam, P.S. Manoharan, Comparative analysis of distributed MPPT controllers for partially shaded stand alone photovoltaic systems, Energy Convers. Manag. 86 (2014) 286–299.
[19] F. Liu, S. Duan, F. Liu, B. Liu, Y. Kang, A variable step size INC MPPT method for PV systems, IEEE Trans. Ind. Electron. 55 (7) (2008) 2622–2628.
[20] Q. Mei, M. Shan, L. Liu, J.M. Guerrero, A novel improved variable step-size incremental-resistance MPPT method for PV systems, IEEE Trans. Ind. Electron. 58 (6) (2011) 2427–2434.
[21] K.S. Tey, S. Mekhilef, Modified incremental conductance MPPT algorithm to mitigate inaccurate responses under fast-changing solar irradiation level, Sol. Energy 101 (2014) 333–342.
[22] S.L. Brunton, C.W. Rowley, S.R. Kulkarni, C. Clarkson, Maximum power point tracking for photovoltaic optimization using ripple-based extremum seeking control, IEEE Trans. Power Electron. 25 (10) (2010) 2531–2540.
[23] P. Lei, Y. Li, J.E. Seem, Sequential ESC-based global MPPT control for photovoltaic array with variable shading, IEEE Trans. Sustain. Energy 2 (3) (2011) 348–358.
[24] A.M. Bazzi, P.T. Krein, Concerning maximum power point tracking for photovoltaic optimization using ripple-based extremum seeking control, IEEE Trans. Power Electron. 26 (6) (2011) 1611–1612.
[25] I. Munteanu, A.I. Bratcu, MPPT for grid-connected photovoltaic systems using ripple-based Extremum Seeking Control: analysis and control design issues, Sol. Energy 111 (2015) 30–42.
[26] M. Orabi, F. Hilmy, A. Shawky, J.A.A. Qahouq, E.-S. Hasaneen, E. Gomaa, On-chip integrated power management MPPT controller utilizing cell-level architecture for PV solar system, Sol. Energy 117 (2015) 10–28.
[27] R. Kotti, W. Shireen, Efficient MPPT control for PV systems adaptive to fast changing irradiation and partial shading conditions, Sol. Energy 114 (2015) 397–407.
[28] A.-A. Bayod-Rújula, J.-A. Cebollero-Abián, A novel MPPT method for PV systems with irradiance measurement, Sol. Energy 109 (1) (2014) 95–104.
[29] J.-A. Jiang, Y.-L. Su, J.-C. Shieh, K.-C. Kuo, T.-S. Lin, T.-T. Lin, W. Fang, J.-J. Chou, J.-C. Wang, On application of a new hybrid maximum power point tracking (MPPT) based photovoltaic system to the closed plant factory, Appl. Energy 124 (2014) 309–324.
[30] J. Ahmed, Z. Salam, A Maximum Power Point Tracking (MPPT) for PV system using Cuckoo Search with partial shading capability, Appl. Energy 119 (2014) 118–130.
[31] K.S. Parlak, FPGA based new MPPT (maximum power point tracking) method for PV (photovoltaic) array system operating partially shaded conditions, Energy 68 (2014) 399–410.
[32] Y.-T. Chen, Z.-H. Lai, R.-H. Liang, A novel auto-scaling variable step-size MPPT method for a PV system, Sol. Energy 102 (2014) 247–256.
[33] S. Daraban, D. Petreus, C. Morel, A novel MPPT (maximum power point tracking) algorithm based on a modified genetic algorithm specialized on tracking the global maximum power point in photovoltaic systems affected by partial shading, Energy 74 (2014) 374–388.
[34] A. Bouilouta, A. Mellit, S.A. Kalogirou, New MPPT method for stand-alone photovoltaic systems operating under partially shaded conditions, Energy 55 (2013) 1172–1185.
[35] H. Fathabadi, Novel high efficient speed sensorless controller for maximum power extraction from wind energy conversion systems, Energy Convers. Manag. 123 (2016) 392–401.
[36] H. Fathabadi, Novel high accurate sensorless dual-axis solar tracking system controlled by maximum power point tracking unit of photovoltaic systems, Appl. Energy 173 (2016) 448–459.
[37] H. Fathabadi, Comparative study between two novel sensorless and sensor based dual-axis solar trackers, Sol. Energy 138 (2016) 67–76.
[38] H. Fathabadi, Fuel cell/back-up battery hybrid energy conversion systems: dynamic modeling and harmonic considerations, Energy Convers. Manag. 103 (2015) 573–584.
[39] D. Molognoniab, S. Puigb, M.D. Balaguerb, A. Liberalec, A.G. Capodaglioa, A. Callegaria, J. Colprimb, Reducing start-up time and minimizing energy losses of Microbial Fuel Cells using maximum power point tracking strategy, J. Power Sources 269 (2014) 403–411.
[40] C. Erbay, S. Carreon-Bautista, E. Sanchez-Sinencio, A. Han, High performance monolithic power management system with dynamic maximum power point tracking for microbial fuel cells, Environ. Sci. Technol. 48 (23) (2014) 13992–13999.
[41] J. Jiao, Maximum power point tracking of fuel cell power system using fuzzy logic control, EEA - Electroteh. Electron. Autom. 62 (2) (2014) 45–52.
[42] M. Zhang, T. Yan, J. Gu, Maximum power point tracking control of direct methanol fuel cells, J. Power Sources 247 (2014) 1005–1010.
[43] N.H. Saad, A.A. El-Sattar, A.E.-A.M. Mansour, Adaptive neural controller for maximum power point tracking of ten parameter fuel cell model, J. Electr. Eng. 13 (3) (2013) 233–239.
[44] J. Jiao, X. Cui, A real-time tracking control of fuel cell power systems for maximum power point, J. Comput. Inf. Syst. 9 (5) (2013) 1933–1941.
[45] N. Karami, R. Outbib, N. Moubayed, Maximum power point tracking with reactant flow optimization of proton exchange membrane fuel cell, J. Fuel Cell Sci. Technol. 10 (5) (2013), 14 pages.
[46] J.-D. Park, Z. Ren, Hysteresis controller based maximum power point tracking energy harvesting system for microbial fuel cells, J. Power Sources 205 (2012) 151–156.
[47] N. Degrenne, F. Buret, B. Allard, P. Bevilacqua, Electrical energy generation from a large number of microbial fuel cells operating at maximum power point electrical load, J. Power Sources 205 (2012) 188–193.
[48] T.F. El-Shatter, M.N. Eskandar, M.T. El-Hagry, Hybrid PV/fuel cell system design and simulation, Renew. Energy 27 (3) (2002) 479–485.
[49] H. Fathabadi, Novel high efficiency DC/DC boost converter for using in photovoltaic systems, Sol. Energy 125 (2016) 22–31.
[50] H. Fathabadi, Power distribution network reconfiguration for power loss minimization using novel dynamic fuzzy c-means (dFCM) clustering based ANN approach, Int. J. Electr. Power Energy Syst. 78 (2016) 96–107.
[51] H. Fathabadi, Novel filter based ANN approach for short-circuit faults detection, classification and location in power transmission lines, Int. J. Electr. Power Energy Syst. 74 (2016) 374–383.
[52] H. Fathabadi, Two novel proposed discrete wavelet transform and filter based approaches for short-circuit faults detection in power transmission lines, Appl. Soft Comput. 36 (2015) 375–382.
[53] H-1000 PEM Fuel Cell Stack User Manual, Horizon fuel cell technologies Co, Aug. 2013.